HEAT TRANSFER ENHANCEMENT INVESTIGATION IN JET IMPINGEMENT SYSTEM OF A SINGLE AND ARRAY OF SQUARE JETS USING NUMERICAL TOOLS

Usman Allauddin,[1,*] Muhammad U. Sohail,[2] Muhammad Sohaib,[1] Mohammad A. Siddiqui,[1] Muhammad H.U. Khan,[1] Kashif Khan,[1] & Patrick G. Verdin[3]

[1]*Mechanical Engineering Department, NED University of Engineering & Technology, Karachi 75270, Pakistan*

[2]*Department of Aeronautics & Astronautics Engineering, Institute of Space Technology (IST), Islamabad, Pakistan*

[3]*Energy & Power, School of Water, Energy & Environment, Cranfield University, Cranfield MK43 0AL, UK*

*Address all correspondence to: Usman Allauddin, Mechanical Engineering Department, NED University of Engineering & Technology, Karachi 75270, Pakistan; Tel.: +00922199261261; Fax: +00922199261255, E-mail: usman.allauddin@neduet.edu.pk

Original Manuscript Submitted: 10/24/2022; Final Draft Received: 1/7/2023

Computational fluid dynamics (CFD) techniques can predict complex fluid flow structures and the thermal performance of jet impingement systems. Numerical studies can complement extensive and time-consuming experimental studies where local parameter measurements are difficult and costly to obtain. In the current work, a combination of one, four, and nine square jets impingements are numerically investigated with CFD for mass flow rate (m) ranging from 2.71 × 10^{-4} to 7.40 × 10^{-4} kg/s. The effects of the jet's outlet-to-target plate distance (Z) are assessed as a function of the width of a single square nozzle (B). The flow field features of different nozzle configurations are also studied. It is shown that the Nusselt number increases as the mass flow rate increases, but increases inversely as the dimensionless jet's outlet-to-target plate spacing Z/B increases. The numerical investigation also demonstrates that when increasing the number of nozzles under a constant mass flow rate, the Nusselt number significantly increases. The effect of nozzle configuration is not that significant at Z/B > 7. It is found that the present impinging jet system offers about 63% enhancement in thermal efficiency, while the pumping power increases by 3.7 times. All simulations are successfully validated with experimental data.

KEY WORDS: *jet impingement, square jet, heat transfer, turbulence modeling, RANS*

1. INTRODUCTION

Impinging jets are extensively used in a wide variety of practical applications due to their simple design and low cost (Cho et al., 2011; Tamir and Kitron, 1987; Bunker et al., 2014; Xie et al., 2018; Agarwal, 2018). Typical applications include the cooling of electronic equipment like CPU and electronic chips, different components of gas turbines, metals, textile products, etc. The recent industrial advancements requiring higher rates of heat transfer from a target surface have generated a need to increase the thermal performance of impinging jet cooling systems. Many parameters can affect the performance of impinging jets such as jet Reynolds number (*Re*), a jet's outlet-to-target plate distance (*Z*), surface roughness, surface temperature, jet arrangements, incidence angle, and fluid properties (Viskanta, 1993; Garimella and Nenaydykh, 1996; Singh et al., 2015; San and Chen, 2014; Singh and Ekkad, 2017; Gori and Petracci,

NOMENCLATURE

B	width of the single square nozzle [m]	X/B	dimensionless axial distance
k_f	fluid thermal conductivity [$Wm^{-1}K^{-1}$]	y^+	y plus – dimensionless number
k_T	turbulent kinetic energy [m^2s^{-2}]	Z	jet's outlet-to-target plate distance [m]
k_L	laminar kinetic energy [m^2s^{-2}]	Z/B	dimensionless jet's outlet-to-target plate distance
m	mass flow rate [kgs^{-1}]		
Nu	Nusselt number	**Greek symbols**	
P	pressure [Pa]	α	thermal diffusivity [m^2s^{-1}]
q	heat flux [Wm^{-2}]	μ	dynamic viscosity [Pa s]
Re	Reynolds number	ϑ	kinematic viscosity [m^2s^{-1}]
T	temperature [K]	ρ	density [kg m^{-3}]
T_{avg}	impingement surface averaged temperature [K]	φ	flow area ratio
		ω	specific dissipation rate [s^{-1}]
T_j	jet temperature [K]		
T'	fluctuating component of T [K]	**Subscripts**	
t	time [s]	$(.)_L$	laminar
U	bulk velocity [ms^{-1}]	$(.)_T$	turbulent
U'	fluctuating component of U [ms^{-1}]	$(.)_j$	jet
X	axial distance [m]	$(.)_{avg}$	averaged

2013). The thermal performance of an impinging jet system can also be increased by using the available jet area effectively. The available jet area can be meshed to convert a single jet impingement into multiple jet impingements. This modification leads to an enhancement of the thermal and flow features of the impinging jet system. The aforementioned method is the core focus of the current study.

A variety of flow configurations are studied in simple impinging jet systems (Sharif, 2016; Li et al., 2009; Akdag et al., 2017; Dutta and Chattopadhyay, 2021). The nozzle geometry can have diverse effects on the heat transfer of impinging jets. Many researchers numerically and experimentally examined the impacts of the nozzle shape, size, aspect ratio, etc. Gulati et al. (2009) studied the impinging jet performance with three differing nozzle shapes. They observed that in the case of a rectangular jet, the thermal performance was enhanced as compared to circular and square jets. They also noted that the pressure loss was the lowest for the circular jet. Singh et al. (2015) investigated the cooling performance of a pipe with different nozzle shapes. The rectangular nozzle provided higher rates of heat transfer in comparison to circular and square nozzles of equal hydraulic diameter and Reynolds number in the range of 10,000 to 25,000. Royne and Dey (2006) used four different configurations, namely a long straight nozzle, short straight nozzle, sharp edge nozzle, and counter sunk nozzle. They found that a higher heat transfer was obtained for a jet generated from a sharp edge nozzle, and a small pressure drop was experienced by the jet from the countersunk nozzle. Chevron jets were used by Alshelahi et al. (2019), and results showed Nusselt number enhancement compared to circular jets due to the turbulence generated by the chevrons. Also, the authors showed that the Nusselt number increased with increasing values of *Re* at different angles and nozzle-to-plate distances. Lyu et al. (2019) investigated the performance of a chevron-shaped jet impingement system used for the thermal cooling of a concave surface. The chevron-shaped nozzle offered 20–30% and 10–15% enhancement in the thermal performance at the small and large jet-to-plate distances, respectively. The effect of the nozzle shape on impingement pressure was investigated by Huang et al. (2020) in a recent study. The jet pressure distribution and jet shape were compared with circular, square, triangular, cross-shaped, and elliptical-shaped nozzles. The peak pressure was found to be the largest with a circular-shaped nozzle. Zhao et al. (2007) compared the performance of a circular impinging jet with square, elliptical, and rectangular-shaped

jets in terms of fluid flow characteristics and surface heat transfer. The authors reported higher thermal performance with the non-circular-shaped impinging jets than with the circular-shaped ones. Vinze et al. (2016) and Almutairi et al. (2019) also studied the nozzle shape to obtain enhanced heat transfer parameters of the jet impingement systems.

The literature survey shows that a significant enhancement in the thermal efficiency of heat exchange devices based on jet impingement can be obtained using non-circular-shaped nozzles. To the authors' best knowledge, among the non-circular-shaped impinging jets studies reported in the open literature, relatively fewer works tackle the flow and thermal performance of square impinging jet systems. Tommaso and Nino (2016) studied the flow structures of a square jet impingement system. The cooling performance of an isothermal plate was studied at different values of the jet's outlet-to-target plate distance. It was observed that the wall-jet flow dominated the flow field at low values of the jet's outlet-to-target plate distance, while at high values, the coherent vortex-induced with the movement of the warm gas significantly disturbed the wall jet flow at the target plate. Tay et al. (2017) investigated the velocity field structure of a horizontal square jet interacting with a free surface. Chuwattanakul et al. (2017) reported enhanced thermal performance of an air jet impingement system with a square-shaped nozzle compared to the one obtained with a circular nozzle. It was observed that the corners of the square nozzle induced recirculation, which in turn brought more turbulence in the flow as compared to the circular jet. Issa and Ortega (2006) experimentally investigated the velocity field and thermal characteristics of a square jet impinging on pin-fins roughened target plates. The thermal performance was found to be increasing with increasing Reynolds number and density of pin-fins. An array of multiple square jets impingement systems was also investigated by different researchers. Weigand and Spring (2011) reviewed multiple jets impingement studies. One method to obtain an array of square jets is to use a wire mesh. Muvvala et al. (2017a) experimentally studied the arrays of square jets produced with three different types of wire mesh. The thermal performance was studied for two different variations: fixed mass flow rate and fixed pumping power. The effect of the jet's outlet-to-target plate distance on the thermal performance was also studied. The wire mesh acted as a turbulence inducer and produced enhanced thermal performance at low values of the jet's outlet-to-target plate distance. The enhanced thermal performance with a wire mesh was also reported in the experimental investigations of Zhou and Lee (2004), Zhou (2005), and Zhou et al. (2006). Similar findings were reported by Muvvala et al. (2017b) who experimentally studied the thermal performance and required pumping powers for varying the jet nozzle conditions. They compared the thermal performance of an array of four and nine square impinging jets with a single square nozzle, keeping the available jet area constant. The averaged *Nu* trends were compared with different combinations of Z/B and m. The turbulence intensity and thermal performance were increased by 140% and 63%, respectively, at a fixed mass flow rate for the multiple nozzles impingement configurations. At lower values of the jet's outlet-to-target plate distance, a 48% maximum decline in pumping power was observed at a fixed heating load.

The literature survey showed that the thermal enhancement of an impinging jet system depends on several parameters. There is a vast amount of literature available on circular jet impingement systems; however, only a few researchers have performed extensive investigations on square jet impingement systems. To the best of the authors' knowledge, no numerical investigation has been reported to date in the open literature regarding the flow and thermal performance of multiple square jets impingement and compared with a single square jet. The current study aims to cover this research gap. In the current work, three-dimensional Reynolds-averaged Navier Stokes (RANS) simulations are performed to investigate the local and averaged thermal and fluid flow parameters with single, four, and nine square jets with the constant jet area. The numerical simulations are based on the experimental setup described in Muvvala et al. (2017b) using the Transition k–kl–ω turbulence model. In Section 4, it is shown that the predicted numerical results match well with the experimentally measured data. The Reynolds number and mass flow rate values used in the current work are reported in Table 1. The geometrical parameters of nozzles for different cases are tabulated in Table 2.

2. SET OF GOVERNING EQUATIONS

The solution of governing equations is obtained employing a steady RANS method in ANSYS FLUENT:

$$\frac{\partial U_i}{\partial x_i} = 0, \tag{1}$$

TABLE 1: Flow parameters for different nozzle configurations

Mass flow rate × 10^{-4} (kg/s)	Reynolds number $Re = m/\varphi B\mu$		
	1 nozzle	4 nozzles	9 nozzles
2.71	3,164	4,637	7,439
4.39	5,120	7,503	12,038
7.40	8,630	12,646	20,289

TABLE 2: Geometric detail of nozzles

Jet configuration	Jet width (mm)	Effective jet flow area (mm^2)	Flow area ratio (φ)
Single nozzle	4.6	21.16	1.00
Four nozzles	1.9	14.44	0.682
Nine nozzles	1.0	9.00	0.425

$$\frac{\partial\left(\rho U_j U_i\right)}{\partial x_j} = -\frac{\partial P}{\partial x_i} + \frac{\partial}{\partial x_j}\left[\mu\left(\frac{\partial U_i}{\partial x_j} + \frac{\partial U_j}{\partial x_i}\right) - \rho\overline{U_i' U_j'}\right], \tag{2}$$

$$\frac{\partial\left(\rho U_i T\right)}{\partial x_i} = \frac{\partial}{\partial x_i}\left[k\frac{\partial T}{\partial x_i} - \rho C_p\overline{U_i' T'}\right]. \tag{3}$$

In RANS modeling, the choice of turbulence model plays a critical role in accurate modeling of the actual flow and thermal physics of jet impingement systems. Many researchers have extensively investigated the performance of available turbulence models in predicting the correct behaviors of impinging jet systems (Zuckerman and Lior, 2006; Hofmann et al., 2007; Alimohammdi et al., 2014; Petera, 2015; Bode et al., 2014). The boundary layer in the wall jet regions undergoes a transition from laminar to turbulent. The correct modeling of this transition is very important to correctly predict the heat transfer taking place at the target plate. Hofmann et al. (2007) investigated the best turbulence model for impinging jets by analyzing the performance of 13 commonly utilized turbulence models. The authors reported the SST *k*–ω model with transition feature as the best turbulence model offering accurate thermal performance in the wall jet flow region. Alimohammdi et al. (2014) and Petera (2015) also reported the good output of SST *k*–ω turbulence model with transition flow feature in predicting the secondary peak of the local Nusselt number distribution. Bode et al. (2014) investigated the performance of six different turbulence models and reported that the Transition *k*–*kl*–ω turbulence model was good in predicting the maximum values of shear rates. Thus, in the current work, the turbulence modeling is performed through the transition *k*–*kl*–ω turbulence model. Readers are referred to ANSYS (2016) for a detailed explanation and a complete set of equations for this model.

3. NUMERICAL SETUP

The computational domains used for different nozzle configurations are a single square jet, four square jets, and nine square jets, as shown in Fig. 1. The gross jet area at the inlet of the nozzle is 4.6 mm × 4.6 mm. The available jet area of a single nozzle is divided to generate different nozzle configurations, increasing the turbulence level in the flow field. The geometries are prepared using the commercial software design modeler available in ANSYS Workbench 16.0.

As shown in Fig. 1, the computational domain exhibits symmetry in the transverse direction, thus a symmetry boundary condition is used at the middle plane to reduce the computational effort. A symmetry boundary condition

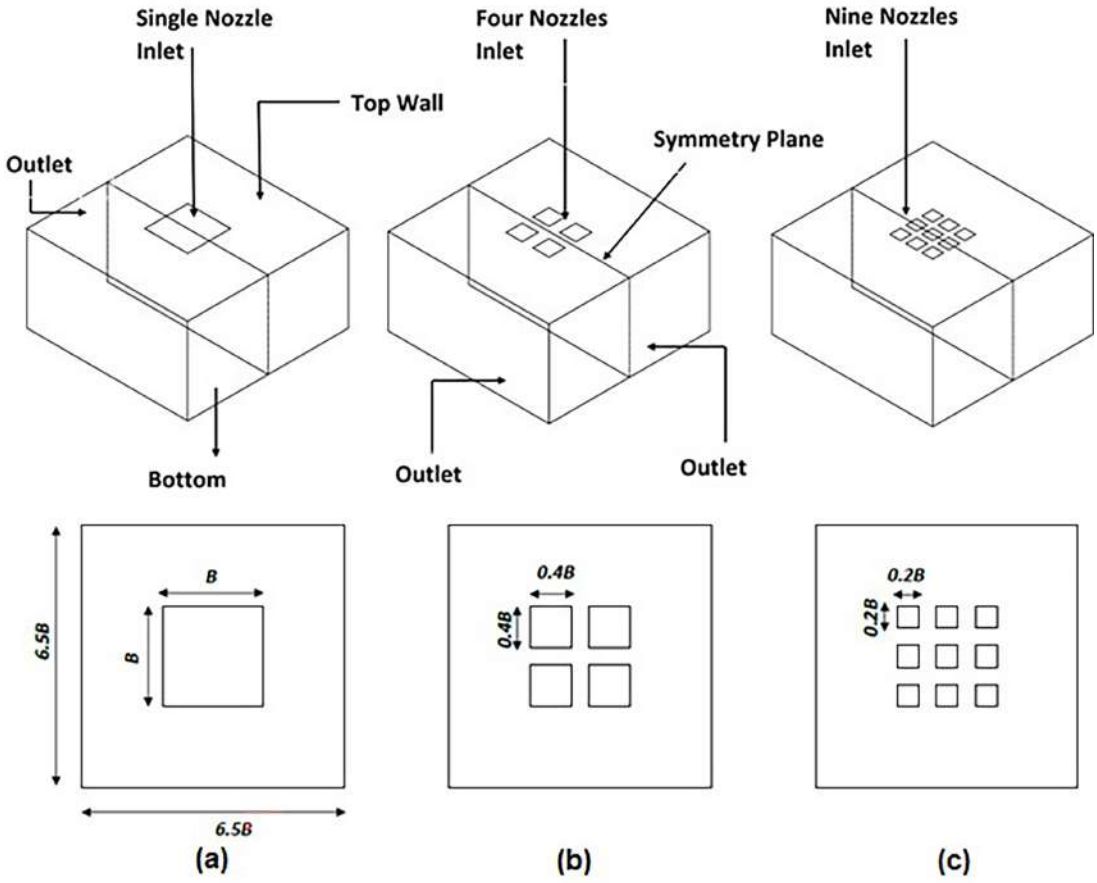

FIG. 1: Computational domain schematic views for (a) single square jet; (b) four square jets; and (c) nine square jets

allows a reduction in the computational domain with the option of using a relatively finer mesh. An inflation layer is applied at the target plate to capture the boundary layer within the wall jet zone. The target plate, modeled with a constant heat flux wall boundary condition, is set up at 5555.55 W/m^2. A velocity-inlet boundary condition is considered with a temperature of 300 K and a turbulence intensity of 5%. An adiabatic wall boundary condition with a no-slip condition is considered on the top surface where the nozzles are located. The remaining surfaces are modeled using a pressure outlet boundary condition to allow backflow during the solution.

The semi-implicit method for pressure-linked equations (SIMPLE) is selected for the pressure-velocity coupling, and second-order schemes are applied for the discretization of all the governing equations. Steady simulations are performed in this work, ignoring body forces, and a 10^{-6} convergence criterion is applied for all equations.

The Nusselt number is calculated as:

$$Nu = \frac{qB}{\left(T_{wall} - T_j\right)k_f}, \tag{4}$$

where, q, B, T_{wall}, T_j, and k_f represent the wall heat flux, nozzle width, wall temperature, jet inlet temperature, and thermal conductivity of the working fluid, respectively.

4. MESH INDEPENDENCE STUDY

The meshing utility available in ANSYS Workbench 16.0 is used to generate the tetrahedrons unstructured meshes of the computational domain. Figure 2 shows a schematic view of the coarse mesh used for the simulation of four nozzles cases at $Z/B = 9$. The medium or fine grid schematic views can't be shown because of the very dense mesh showing only black regions in the domain. In the current work, the grid convergence index (GCI) technique by Celik et al. (2008) is used to quantify the numerical errors caused by insufficient space discretization. A mesh independence study is performed for the cases of a single jet and an array of four square jets. For both configurations, a mass flow rate of 2.71×10^{-4} kg/s is considered with a jet outlet-to-target wall distance $Z/B = 9$. Three systematically refined meshes of around 0.94 million, 2.6 million, and 6.7 million elements are prepared, ensuring the non-dimensional wall normal distance y^+ remains less than 1.0. The mesh details and the averaged Nusselt number values at the target plate with all meshes are reported in Table 3. The GCI values are found to be 2.25% and 3.22% for the single jet and array of four jet cases, respectively. It is established that the mesh comprising around 2.6 million elements is suitable for further study, as only a slight difference in results is obtained with the medium and fine meshes.

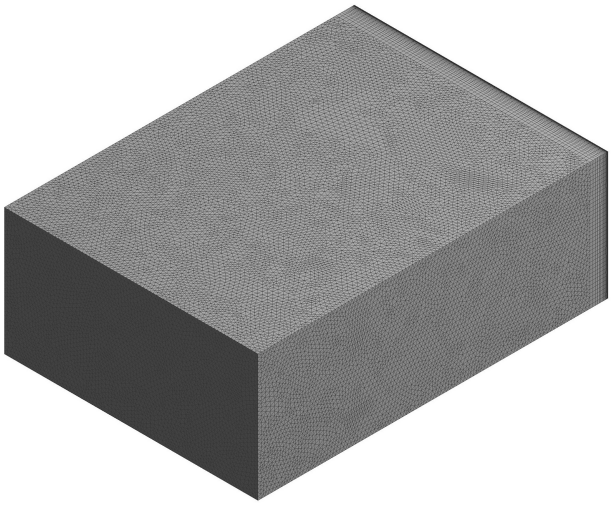

FIG. 2: Coarse mesh view for four nozzles' configuration at $Z/B = 9$

TABLE 3: Grid independence study for single and four nozzle configurations at $Z/B = 9$ and $m = 2.71 \times 10^{-4}$ kg

	Coarse grid	Medium grid	Fine grid
Elements	939156	2610204	6659595
Nodes	216928	518093	1350188
y^+	0.5	0.43	0.40
Single nozzle configuration			
$N_{u,avg}$	22.185	23.45	23.81
GCI_{fine}	—	2.25%	—
Four-nozzle configuration			
$N_{u,avg}$	25.39	26.37	26.82
GCI_{fine}	—	3.22%	—

5. RESULTS AND DISCUSSION

In this section, the flow field and heat transfer results are discussed for a mass flow rate of 2.71×10^{-4} to 7.40×10^{-4} kg/s and normalized jet's outlet-to-target plate distance (Z/B) of 2 to 9. First, the effect of different nozzle configurations on flow fields is analyzed. The flow field results are analyzed at a fixed mass flow rate of 2.71×10^{-4} kg/s, while Z/B values are varied from 2 to 9 for all nozzle configurations. Second, the effect of different nozzle configurations on turbulent kinetic energy distribution is analyzed. Last, the heat transfer performance is analyzed at different nozzle configurations. The heat transfer results are analyzed at different combinations of the input parameters.

5.1 Flow Field Results

Flow and turbulent kinetic energy field results are discussed in this section. The study of flow and turbulent kinetic energy fields is important, not only to study the flow and turbulence characteristics, but also to better understand the heat transfer results. Figures 3–5 illustrate the local flow field at constant mass flow rate $m = 2.71 \times 10^{-4}$ kg/s for a single jet, four jets, and nine jets configuration, respectively. It can be seen that the impinging jets at the nozzle outlet have a uniform velocity profile for all nozzle configurations. The potential core region, which is characterized by having velocity values equal to the nozzle exit velocity, can be seen in Fig. 3. The strength of the jet impact on the target wall decreases with increasing values of Z/B. The stagnation region, which is characterized by having zero velocity regions, also shrinks with increasing values of Z/B. At the downstream end of the potential core, where the jet is approaching the target wall, the velocity profile becomes non-uniform. The magnitude of centerline velocity decreases with an increasing distance from the nozzle exit. As the jet flow approaches the wall, it is decelerated in the wall-normal direction and then accelerated in the wall's transverse direction after going through the stagnation region. It can also be observed in Fig. 3 that there is definite flow acceleration in the wall jet flow region. As the jet continues to intake stationary fluid from the surroundings, the wall jet region begins experiencing deceleration in the transverse direction. It can also be observed that the thickness of the boundary layer formed at the target wall decreases with increasing values of Z/B. This is due to the jet, which approaches the target wall with relatively less velocity at high values of Z/B. Similar trends are observed in Figs. 4 and 5. The most interesting feature is that the potential core is not formed in the cases of four and nine nozzles. It can be observed in Fig. 4 that for the four nozzles configuration, the stagnation region displays a cone shape. It can also be observed that for $Z/B = 2$ and 3.5, the twin jets separately strike the target plate, but for $Z/B = 5$, 7, and 9 the jets merge before impinging onto the target plate. The velocity patterns for the nine nozzle case are similar to the four nozzle case. All the jets merge and impinge as a single jet at $Z/B = 9$. This shows that the effect of nozzle configuration vanishes at high values of Z/B. The comparison of Figs. 3–5 also shows that the magnitude of velocity at the nozzle outlet increases with an increasing number of nozzles for a fixed value of m.

Muvvala et al. (2017b) claimed that an increasing number of nozzles would produce more turbulence compared to a single nozzle flow condition. This, in turn, would produce an enhanced thermal performance as the number of nozzles would be increased. This is discussed and evidenced in the current work through the prediction of the turbulent kinetic energy distribution for different nozzle configurations. The comparison of turbulent kinetic energy for different nozzle configurations with $Z/B = 7$ is shown in Fig. 6. The turbulent kinetic energy values are found to increase with an increasing number of nozzles. Thus, the turbulence level of an impinging jet system can also increase by using the available jet area effectively.

5.2 Thermal Performance of the Cases Studied

The thermal results are discussed in this section. The numerical results are compared with the experimental measurements of Muvvala et al. (2017b). First, the influence of the jet's outlet-to-target plate height on heat transfer performance is analyzed. Figure 7 shows the comparison of averaged Nusselt number versus Z/B ranging from 2 to 9 for all nozzle configurations at a fixed $m = 2.71 \times 10^{-4}$ kg/s. Figures 8 and 9 show the similar comparisons for the mass flow rates of 4.39×10^{-4} kg/s and 7.4×10^{-4} kg/s, respectively. The comparison of numerically predicted and experimentally measured results shows a good validation of the predicted results. It can be seen that the thermal performance decreases with increasing values of Z/B for all nozzle configurations and all values of mass flow rate. The decreasing

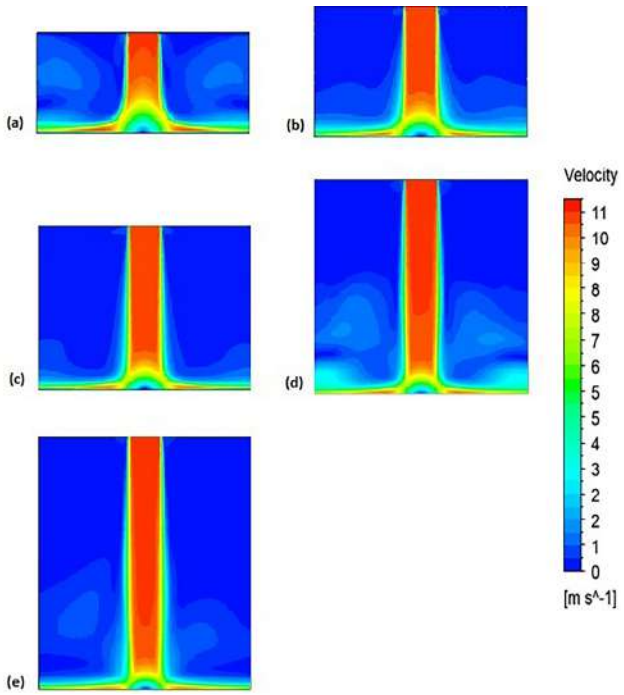

FIG. 3: Velocity contours for the single nozzle configuration at $m = 2.71 \times 10^{-4}$ kg/s for (a) $Z/B = 2$; (b) $Z/B = 3.5$; (c) $Z/B = 5$; (d) $Z/B = 7$; and (e) $Z/B = 9$

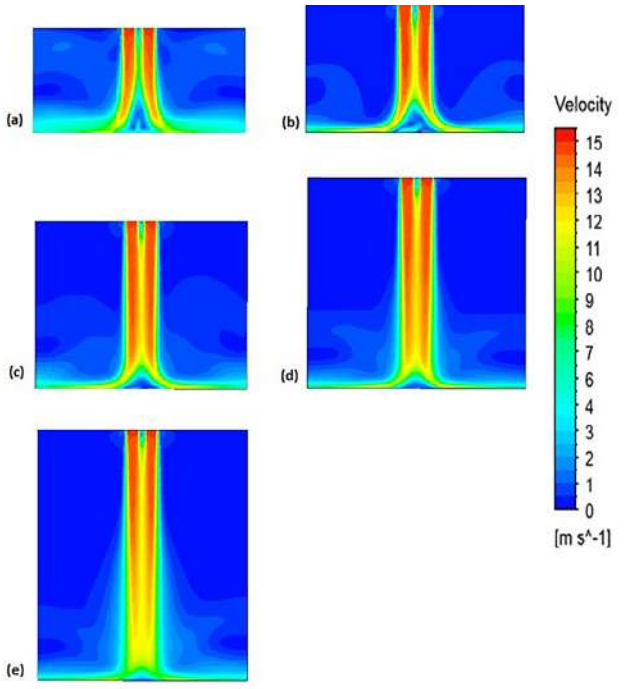

FIG. 4: Velocity contours for the four nozzles' configuration at $m = 2.71 \times 10^{-4}$ kg/s for (a) $Z/B = 2$; (b) $Z/B = 3.5$; (c) $Z/B = 5$; (d) $Z/B = 7$; and (e) $Z/B = 9$

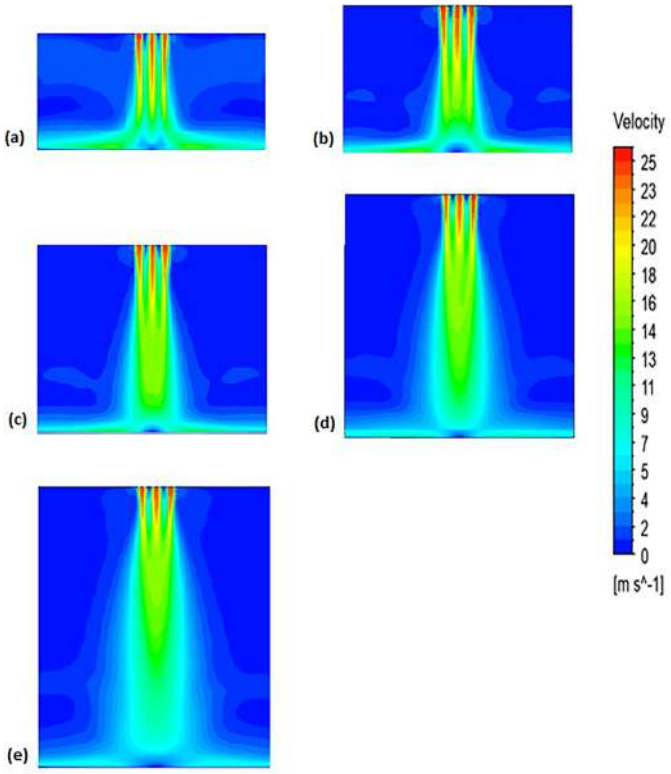

FIG. 5: Velocity contours for the nine nozzles' configuration at $m = 2.71 \times 10^{-4}$ kg/s for (a) $Z/B = 2$; (b) $Z/B = 3.5$; (c) $Z/B = 5$; (d) $Z/B = 7$; and (e) $Z/B = 9$

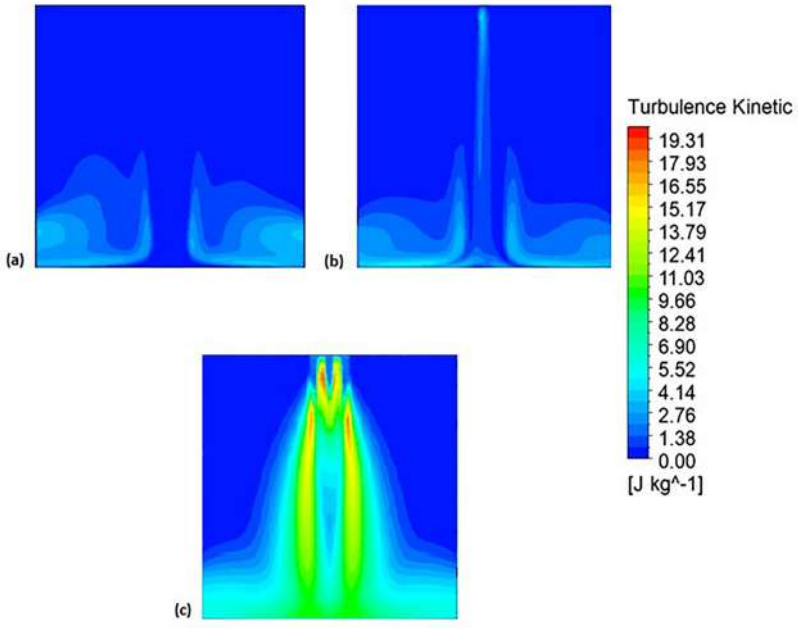

FIG. 6: Turbulent kinetic energy contours at $m = 2.71 \times 10^{-4}$ kg/s and $Z/B = 9$ for (a) 1 nozzle; (b) 4 nozzles; and (c) 9 nozzles

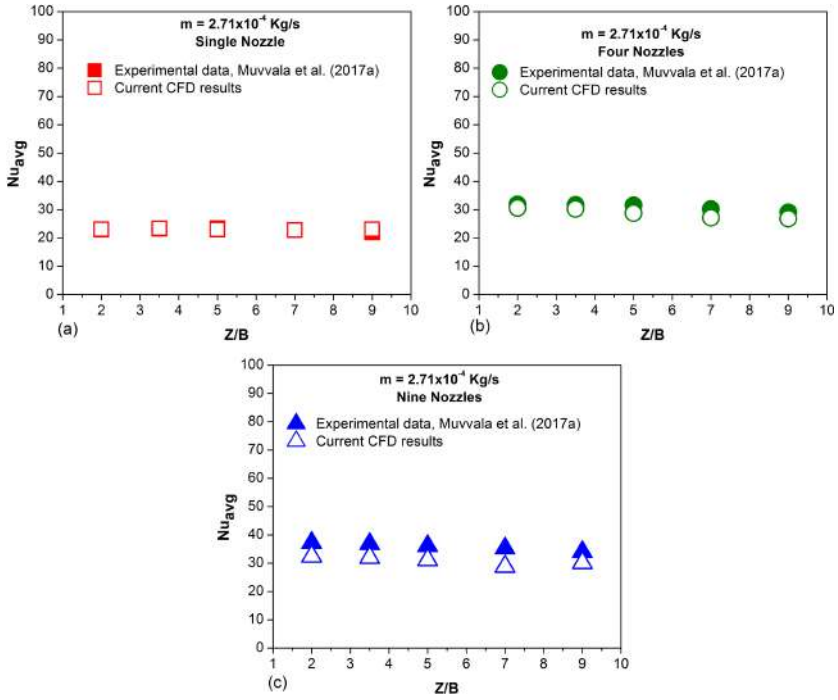

FIG. 7: Averaged Nusselt number versus Z/B plot at $m = 2.71 \times 10^{-4}$ kg/s for (a) single square jet; (b) four square jets; and (c) nine square jets

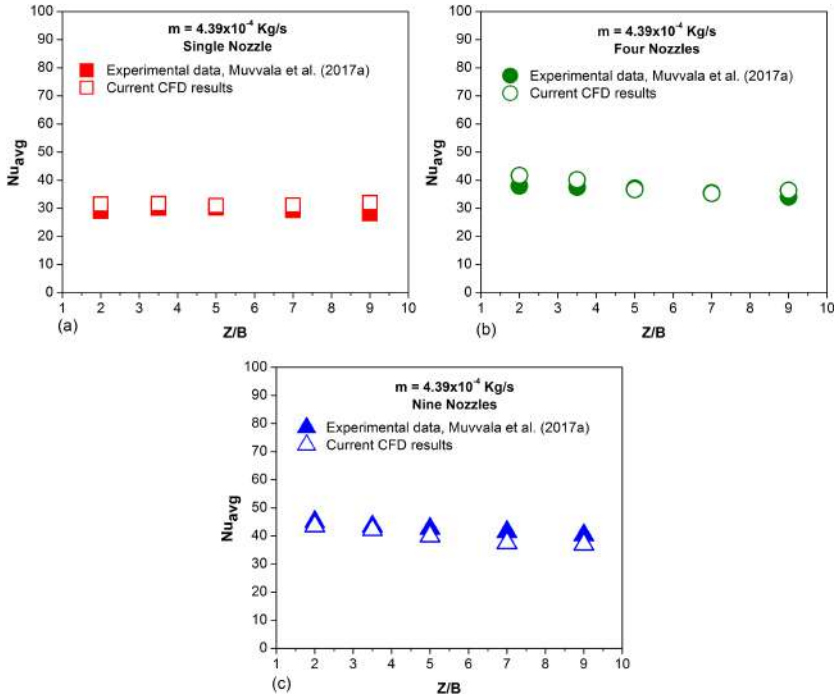

FIG. 8: Averaged Nusselt number versus Z/B plot at $m = 4.39 \times 10^{-4}$ kg/s for (a) single square jet; (b) four square jets; and (c) nine square jets

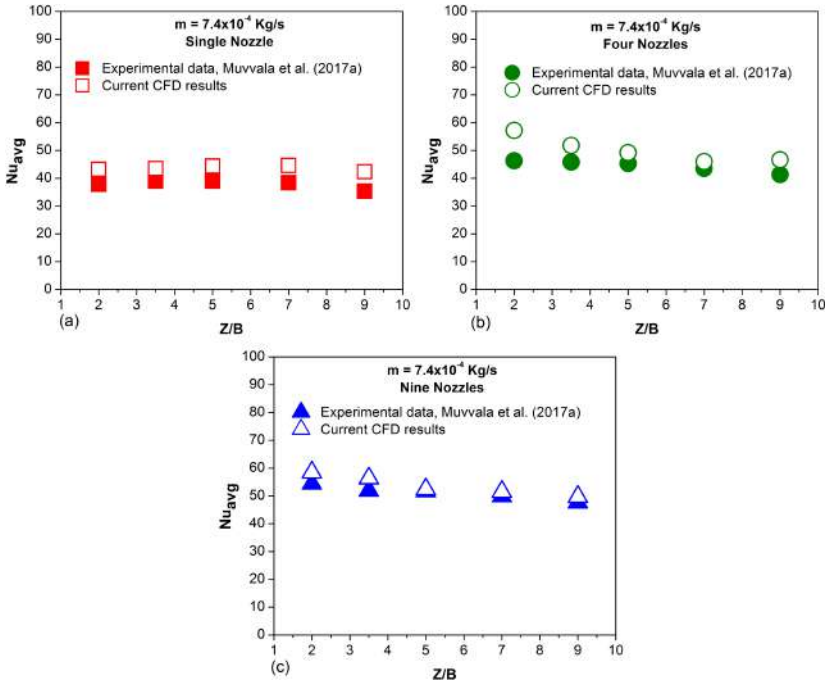

FIG. 9: Averaged Nusselt number versus Z/B plot at $m = 7.4 \times 10^{-4}$ kg/s for (a) single square jet; (b) four square jets; and (c) nine square jets

trend is more prominent in the cases of four and nine nozzles. The enhanced thermal performance using an array of four and nine nozzles can be observed in Figs. 7–9.

Figures 10 and 11 show the influence of m on the thermal results at Z/B of 3.5 and 7, respectively. The averaged Nu values increase with the increasing value of m. The high mass flow rates correspond to high values of the Reynolds numbers. The Nusselt number has a dependence on Reynolds number, thus enhanced thermal performance is observed at high values of mass flow rate. The comparison of Figs. 10 and 11 also shows an enhanced thermal performance with four and nine nozzles cases.

Figure 12 shows the effect of the number of nozzles on the averaged Nu values as Z/B and m increase. The increment in mass flow rate gives a higher heat transfer. It can also be observed that the increasing number of nozzles brings a significant enhancement in the thermal performance, only at low values of Z/B. At high values of Z/B, an enhancement is present, but it is not significant.

The increase of the normalized distance Z/B does not seem to influence highly the averaged Nu in the case of a single nozzle configuration, as the values remain almost constant for each specific mass flow rate investigated. Here it is important to mention that although the thermal performance is increased with the increasing number of nozzles, it is achieved at the expense of increased pumping power. Muvvala et al. (2017b) provided a comparison of heat transfer versus pumping power. For a mixed mass flow rate, about 63% enhancement in the thermal efficiency is found, while the pumping power increases by 3.7 times (Muvvala et al., 2017b). For a fixed heat removal load, the usage of multiple nozzles is advantageous only at low values of Z/B where the pumping power is reduced by 48% (Muvvala et al., 2017b).

6. CONCLUSIONS

A numerical study of the experimental work of Muvvala et al. (2017b) was performed to complement the experimental data by numerically predicting the complex local jet flow structures and thermal performance of a single and multiple jet impingement systems. The mass flow rate was varied from 2.71×10^{-4} to 7.40×10^{-4} kg/s and normalized jet's

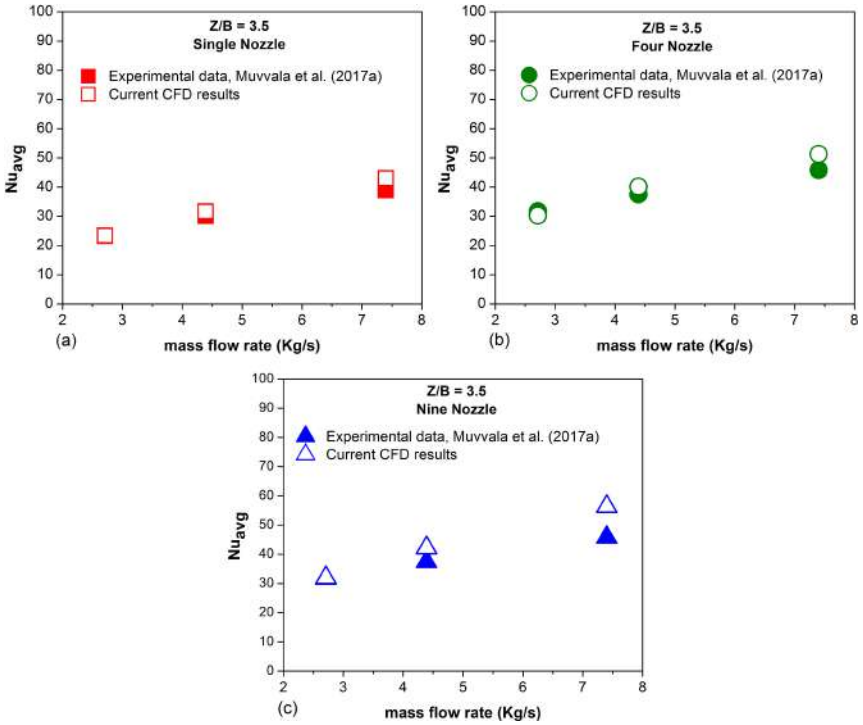

FIG. 10: Averaged Nusselt number versus *m* plot at *Z*/*B* = 3.5 for (a) single square jet; (b) four square jets; and (c) nine square jets

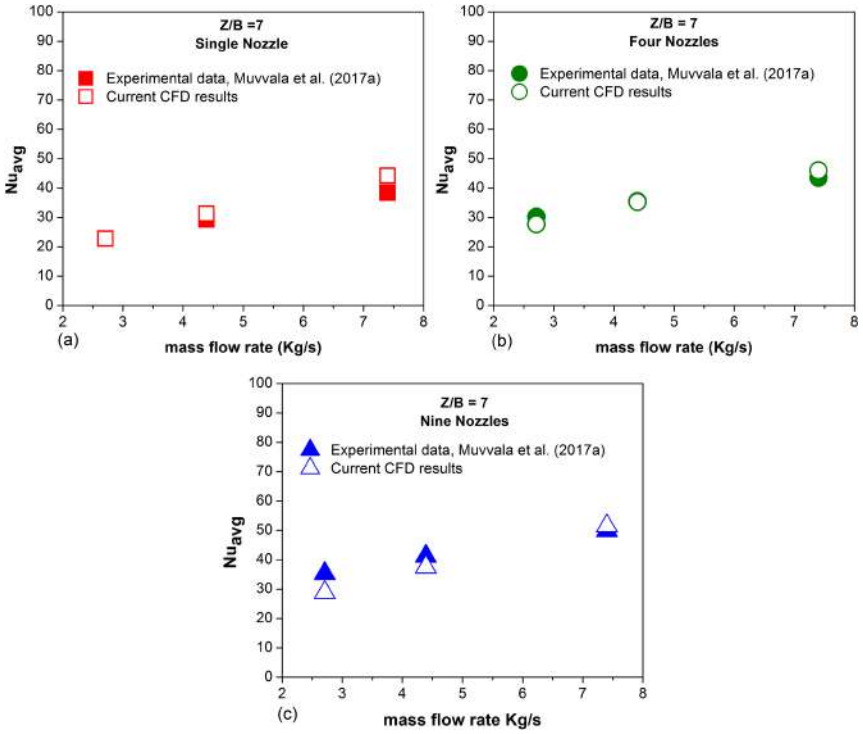

FIG. 11: Averaged Nusselt number versus *m* plot at *Z*/*B* = 7 for (a) single square jet; (b) four square jets; and (c) nine square jets

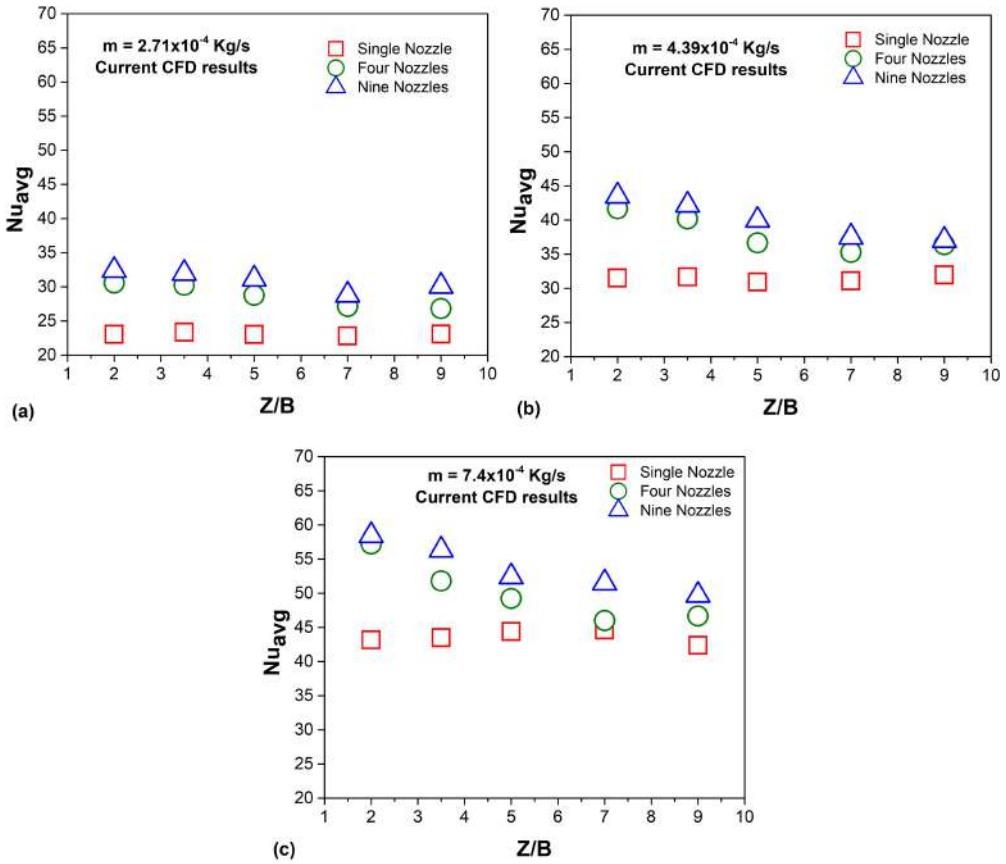

FIG. 12: CFD averaged Nusselt number variation with different Z/B values for (a) $m = 2.71 \times 10^{-4}$ kg/s; (b) $m = 4.39 \times 10^{-4}$ kg/s; and (c) $m = 7.4 \times 10^{-4}$ kg/s

outlet-to-target plate distances Z/B from 2 to 9 were considered. The numerical results were found to be in quite well agreement with the experimentally measured data. The important conclusions of the study are as follows:

- The flow field characteristics of four and nine nozzles configurations are different in terms of the potential core formation. The potential core is not observed in multiple nozzles configurations.
- The multiple nozzle configurations offer increased jet impingement velocities.
- The effect of nozzle conditions vanishes at high values of Z/B.
- The multiple nozzle configurations offer an increased level of turbulence.
- The enhancement in thermal performance can be achieved with multiple nozzle configurations.
- The maximum enhancement with multiple nozzles configurations is observed at low values of Z/B with a reduced pumping power to get a fixed heat removal load.

There is significant potential available to enhance the performance of jet impingement systems. In the current work, a technique based on using the total jet area effectively is used to bring thermal performance enhancement in square jet impinging system, which will eventually help in the development of more compact, lighter, and cheaper cooling systems.

In the future, the authors will investigate the influence of different nanofluids and extended surfaces on the thermal and fluid flow performance of the current impinging jet systems configurations. A detailed parametric study involving different nanoparticles and the variation of extended surfaces' geometric parameters will be conducted. The effect of pulsating jets can also be explored as future research work.

ACKNOWLEDGMENT

This work was funded by NED University of Engineering & Technology, Pakistan, as an Independent Research Project (Grant No. Acad/50(48)/6921).

REFERENCES

Agarwal, C., Surface Quenching by Jet Impingement – A Review, *Steel Res. Int.*, vol. **90**, no. 1, p. 1800285, 2018.

Akdag, U., Akcay, S., and Demiral, D., The Investigation of the Heat Transfer Characteristics of a Cross-Flow Pulsating Jet in a Forced Flow, *Comput. Therm. Sci.: Int. J.*, vol. **9**, pp. 567–582, 2017.

Alimohammadi, S., Murray, D.B., and Persoons, T., Experimental Validation of a Computational Fluid Dynamics Methodology for Transitional Flow Heat Transfer Characteristics of a Steady Impinging Jet, *J. Heat Transf.*, vol. **136**, no. 9, 2014.

Almutairi, M.M.S.M.A., Maghrabie, H.M., Attalla, M., and Fatah, M.A.E., Experimental Study of Impinging Cooling of Flat Surface Utilizing Unconfined Chevron Jets, *J. Sci. Eng. Res.*, vol. **6**, no. 3, pp. 188–195, 2019.

Alshelahi, F.F.M.F., Maghrabie, H.M., and Attalla, M., Effect of Pair Chevron Impinging Jets on Heat Transfer Coefficient, *J. Sci. Eng. Res*., vol. **6**, no. 3, pp. 99–104, 2019.

ANSYS Fluent, ANSYS Fluent User's Guide, ANSYS, Inc., Release 17.2, 2016.

Bode, F., Sodjavi, K., Meslem, A., and Nastase, I., Comparison of Turbulence Models in Simulating a Cruciform Impinging Jet on a Flat Wall, *Proc. of the 15th Int. Heat Transfer Conf.*, Kyoto, Japan, August 10–15, 2014.

Bunker, R.S., Dees, J.E., and Palafox, P., Impingement Cooling in Gas Turbines: Design, Applications, and Limitations, *WIT Trans. State Art Sci. Eng*., vol. **76**, 2014.

Celik, I.B., Ghia, U., and Roache, P.J., Procedure for Estimation and Reporting of Uncertainty due to Discretization in CFD Applications, *J. Fluid Eng*., vol. **130**, no. 7, 2008.

Cho, H.H., Kim, K.M., and Song, J., Applications of Impingement Jet Cooling Systems, in *Cooling Systems: Energy, Engineering and Applications*, Hauppauge, NY: Nova Science Publishers, Inc., pp. 37–67, 2011.

Chuwattanakul, V., Wongcharee, K., Nanan, K., and Eiamsa-ard, S., Investigation of Heat Transfer of a Square Impinging Air Jet on a Flat Surface Using Thermochromic Liquid Crystal Sheet, in *Materials in Environmental Engineering: Proc. of the 4th Annual Int. Conf. on Materials Science and Environmental Engineering*, Boston, pp. 1385–1394, 2017.

Dutta, P. and Chattopadhyay, H., Numerical Analysis of Transport Phenomena under Turbulent Annular Impinging Jet, *Comput. Therm. Sci.: Int. J.*, vol. **13**, pp. 1–19, 2021.

Garimella, S.V. and Nenaydykh, B., Nozzle-Geometry Effects in Liquid Jet Impingement Heat Transfer, *Int. J. Heat Mass Transf*., vol. **39**, no. 14, pp. 2915–2923, 1996.

Gori, F. and Petracci, I., On the Effect of the Slot Height in the Cooling of a Circular Cylinder with a Rectangular Jet, *Int. Commun. Heat Mass Transf.*, vol. **48**, pp. 8–14, 2013.

Gulati, P., Katti, V., and Prabhu, S.V., Influence of the Shape of the Nozzle on Local Heat Transfer Distribution between Smooth Plate Surface and Impinging Air Jet, *Int. J. Therm. Sci*., vol. **48**, pp. 602–617, 2009.

Hofmann, H.M., Kaiser, R., Kind, M., and Martin, H., Calculations of Steady and Pulsating Impinging Jets—An Assessment of 13 Widely Used Turbulence Models, *Numer. Heat Transf. Part B*, vol. **51**, no. 6, pp. 565–583, 2007.

Huang, F., Mi, J., Li, D., and Wang, R., Impinging Performance of High-Pressure Water Jets Emitting from Different Nozzle Orifice Shapes, *J. Geofluids*, vol. **2020**, 2020.

Issa, J.S. and Ortega, A., Experimental Measurements of the Flow and Heat Transfer of a Square Jet Impinging on an Array of Square Pin Fins, *J. Elect. Pack*., vol. **128**, pp. 61–70, 2006.

Li, D., Li, Timchenko, V., Reizes, J.A., and Leonardi, E., Effect of Operating Frequency on Heat Transfer in a Microchannel with Synthetic Jet, *Comput. Therm. Sci.: Int. J*., vol. **1**, pp. 361–383, 2009.

Lyu, Y., Zhang, J., Liu, X., and Shan, Y., Experimental Study of Single-Row Chevron-Jet Impingement Heat Transfer on Concave Surfaces with Different Curvatures, *Chin. J. Aeronaut.*, vol. **32**, no. 10, pp. 2275–2285, 2019.

Muvvala, P., Balaji, C., and Venkateshan, S.P., Experimental Investigation on Heat Transfer from Square Jets Issuing from Perforated Nozzles, *Heat Mass Transf*., vol. **53**, pp. 2363–2375, 2017a.

Muvvala, P., Balaji, C., and Venkateshan, S.P., Experimental Investigation on the Effect of Wire Mesh at the Nozzle Exit on Heat Transfer from Impinging Square Jets, *Exp. Therm. Fluid Sci.*, vol. **84**, pp. 78–89, 2017b.

Petera, K., Turbulent Heat Transport and Its Anisotropy in an Impinging Jet, *EPJ Web Conf.*, vol. **92**, p. 02063, 2015.

Royne, A. and Dey, C.J., Effect of Nozzle Geometry on Pressure Drop and Heat Transfer in Submerged Jet Arrays, *Int. J. Heat Mass Transf*., vol. **49**, pp. 800–804, 2006.

San, J.Y. and Chen, J.J., Effects of Jet-to-Jet Spacing and Jet Height on Heat Transfer Characteristics of an Impinging Jet Array, *Int. J. Heat Mass Transf*., vol. **71**, pp. 8–17, 2014.

Sharif, M.A.R., Numerical Investigation of Round Turbulent Swirling Jet Impingement Heat Transfer from a Hot Surface, *Comput. Therm. Sci.: Int. J.*, vol. **8**, pp. 489–507, 2016.

Singh, D., Premachandran, B., and Kohli, S., Effect of Nozzle Shape on Jet Impingement Heat Transfer from a Circular Cylinder, *Int. J. Therm. Sci*., vol. **96**, pp. 45–69, 2015.

Singh, P. and Ekkad, S.V., Effects of Spent Air Removal Scheme on Internal-Side Heat Transfer in an Impingement-Effusion System at Low Jet-to-Target Plate Spacing, *Int. J. Heat Mass Transf*., vol. **108**, pp. 998–1010, 2017.

Tamir, A. and Kitron, A., Applications of Impinging-Streams in Chemical Engineering Processes—Review, *Chem. Eng. Commun.*, vol. **50**, nos. 1–6, pp. 241–330, 1987.

Tay, G.F.K., Rahman, M.S., and Tachie, M.F., Characteristics of a Horizontal Square Jet Interacting with the Free Surface, *Phys. Rev. Fluids*, vol. **2**, 2017.

Tommaso, R.M.D. and Nino, E., Investigation on an Impinging Square Jet, *Int. J. Modern Eng. Res.*, vol. **7**, no. 10, 2016.

Vinze, R., Chandel, S., Limaye, M.D., and Prabhu, S.V., Influence of Jet Temperature and Nozzle Shape on the Heat Transfer Distribution between a Smooth Plate and Impinging Air Jets, *Int. J. Therm. Sci*., vol. **99**, pp. 135–151, 2016.

Viskanta, R., Heat Transfer to Impinging Isothermal Gas and Flame Jets, *Exp. Therm. Fluid Sci.*, vol. **6**, no. 2, pp. 111–134, 1993.

Weigand, B. and Spring, S., Multiple Jet impingement – A Review, *Heat Transf. Res.*, vol. **42**, no. 2, pp. 101–142, 2011.

Xie, R., Wang, H., Xu, B., and Wang, W., A Review of Impingement Jet Cooling in Combustor Liner, *Proc. of Turbo Expo: Power for Land, Sea and Air*, Oslo, Norway, GT2018-76335, 2018.

Zhou, D.W. and Lee, S.J., Heat Transfer Enhancement of Impinging Jets Using Mesh Screens, *Int. J. Heat Mass Transf*., vol. **47**, pp. 2097–2108, 2004.

Zhou, D.W., Effect of Mesh Screen on Heat Transfer Enhancement of Impinging Jet, *J. Enhanced Heat Transf*., vol. **12**, no. 1, pp. 101–120, 2005.

Zhao, W., Kumar, K., and Mujumdar, A.S., Flow and Heat Transfer Characteristics of Confined Noncircular Turbulent Impinging Jets, *Dry. Technol*., vol. **22**, no. 9, pp. 2027–2049, 2007.

Zhou, D.W., Lee, S.J., Ma, C.F., and Bergles, A.E., Optimization of Mesh Screen for Enhancing Jet Impingement Heat Transfer, *Heat Mass Transf*., vol. **42**, pp. 501–510, 2006.

Zuckerman, N. and Lior, N., Jet Impingement Heat Transfer: Physics, Correlations, and Numerical Modelling, *Adv. Heat Transf*., vol. **39**, pp. 565–631, 2006.